Supplementary Materials: Nonmonotonic diffusion in crowded environments

Gregory Garbès Putzel, Mario Tagliazucchi, and Igal Szleifer

August 14, 2014

1 BD simulation time step

In this work we have used a Brownian Dynamics (BD) simulation time step of

$$dt = 4.5 \times 10^{-4}\tau, \tag{1}$$

where $\tau = r_d^2/6D_0$ is the characteristic time required for a diffusing particle to move a distance equal to its own radius. In this section we show that our choice of time step is sufficiently small for our purposes, as well as showing that our main results are not dependent on our choice of time step.

When the diffusing particle encounters the hard repulsive potential of a crowder, it experiences a large force approximately equal to U_{large}/δ, where $U_{\text{large}} = 40k_BT$ is a large change in potential that occurs over a small distance $\delta = 0.1\,\text{nm}$. In order for our results to be independent of the simulation time step, it is important that the distance travelled by the diffuser during a single time step be smaller than the size of the smallest physical feature in the system, namely the width $\delta = 0.1\,\text{nm}$ of the hard repulsive potential. In each step of a BD simulation, a diffusing particle undergoes a displacement due to both a fluctuating thermal force and to the particle's drift velocity in a potential gradient. We now verify that given our choice of time step, each of these displacements is smaller than δ. The fluctuating force gives rise, in the absence of any obstacles, to the "bare" diffusion coefficient D_0. Therefore the associated typical displacement during a time step is

$$dr^{\text{fluct}} \approx \sqrt{6D_0 dt} = \sqrt{4.5^{-4}} r_d = 0.02\,\text{nm}, \tag{2}$$

which is significantly smaller than $\delta = 0.1\,\text{nm}$. The displacement associated with the drift velocity due to the force U_{large}/δ is

$$dr^{\text{drift}} = v^{\text{drift}} dt = \frac{1}{\gamma}\frac{U_{\text{large}}}{\delta} dt = \frac{D_0}{k_BT}\frac{U_{\text{large}}}{\delta} dt = 0.03\,\text{nm}, \tag{3}$$

which is also significantly smaller than δ. Thus, in our simulations the time step is small enough that the large repulsive forces do not produce spurious results.

We have performed BD simulations with a smaller time step of $dt = 9 \times 10^{-5}\tau$. These simulations were used to calculate the effective diffusion coefficient at the same physical time as in the previous simulations; Fig. 1 shows that the results depend very little on the value of the time step, and that our main result (the non-monotonicity of the diffusion coefficient as a function of the attraction strength ϵ) is independent of the time step.

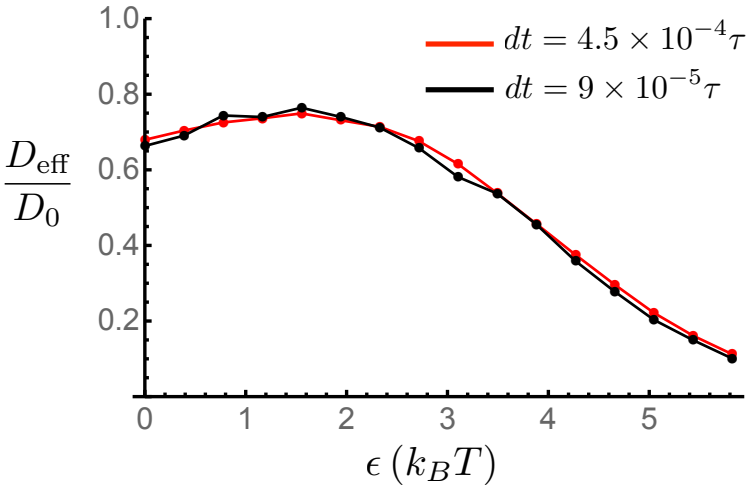

Figure 1: Effective diffusion coefficients calculated from simulations with different BD simulation time steps dt. The crowder volume fraction is $\phi = 0.24$.

Additionally, in Supplementary Materials section 11 we present the results of solving the continuum (Fokker-Planck) diffusion equation associated with a particle diffusing among fixed crowders. This method does not involve any choice of time step, but still shows the same non-monotonic behavior of $D_{\text{eff}}(\epsilon)$.

2 MSD data

In Fig. 2 we show raw data of mean squared displacements (MSD) for three different crowder levels: $\phi = 0.01$, $\phi = 0.24$, and $\phi = 0.40$. Fig. 3 shows the MSD at a particular time ($t = 10^4\,\tau$), highlighting the non-monotonic dependence of diffusion rate on the diffuser-crowder attraction strength ϵ. Figures 4 and 5 show MSD data for short times.

3 Alternative method for calculation of D_{eff}

In addition to the method used in the article (1/6 of the average slope of the MSD curve at long times) we have used an alternative method to calculate diffusion coefficients (1, 2). The logarithm of MSD/6t is plotted against

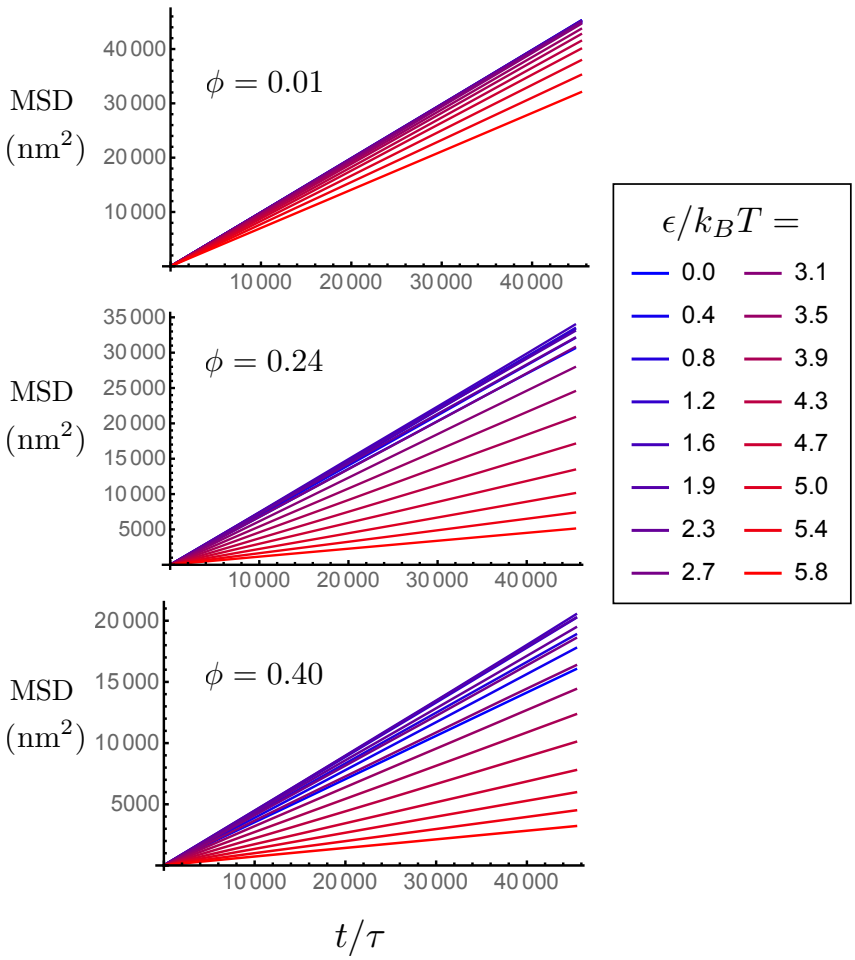

Figure 2: Selected MSD data for three different values of the crowder volume fraction ϕ, and for a range of values of the attraction strength ϵ.

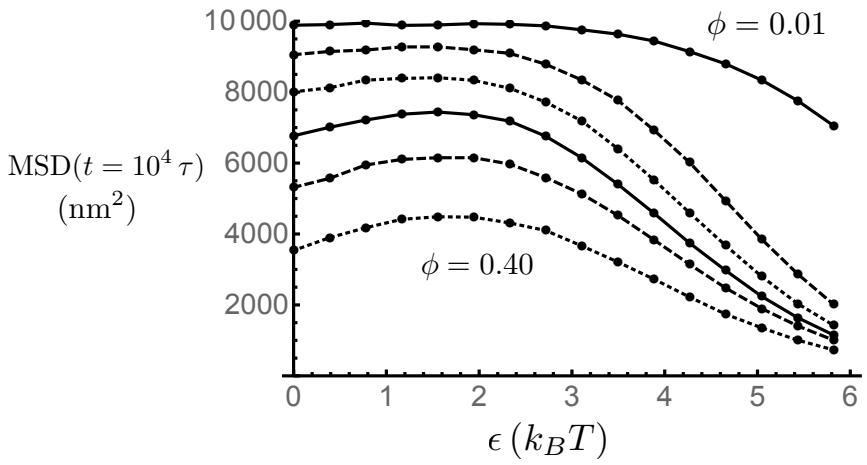

Figure 3: The mean squared displacement of the diffusing particles, evaluated at time $t = 10^4\,\tau$, as a function of the strength ϵ of the crowder-diffuser attractive interaction. This is shown for six different values of the crowder volume fraction. Top to bottom: $\phi = 0.01$, $\phi = 0.08$, $\phi = 0.16$, $\phi = 0.24$, $\phi = 0.32$, and $\phi = 0.40$. Compare to Fig. 2 of the article.

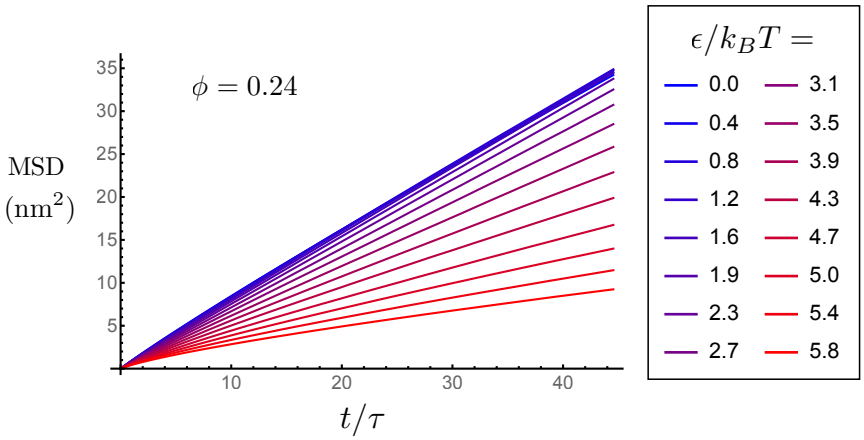

Figure 4: Short-time MSD data for crowder volume fraction $\phi = 0.24$, and for a range of values of the attraction strength ϵ.

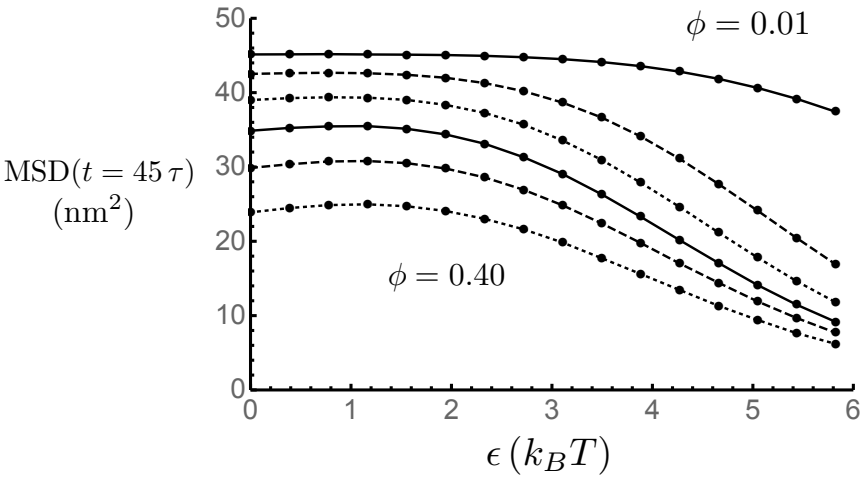

Figure 5: The mean squared displacement of the diffusing particles, evaluated at time $t = 45\,\tau$, as a function of the strength ϵ of the crowder-diffuser attractive interaction. This is shown for six different values of the crowder volume fraction. Top to bottom: $\phi = 0.01$, $\phi = 0.08$, $\phi = 0.16$, $\phi = 0.24$, $\phi = 0.32$, and $\phi = 0.40$

the logarithm of time in Fig. 6 for several values of the the crowder volume fraction, and for a range of crowder-diffuser attraction strengths. This allows one to check visually that the simulations have reached the regime of long-time diffusion, since $\ln(\mathrm{MSD}/6t)$ reaches a plateau value. These plateau values, shown in Fig. 6 as dashed lines, are estimates of $\ln(D_{\mathrm{eff}})$. By taking the exponential of these, we obtain new estimates for D_{eff}. Fig. 7 shows that these new estimates are essentially identical to the ones reported in the article.

4 $\epsilon_{\mathbf{max}}$ for a square well potential

Equation (4) of the article gives the value of ϵ that maximizes the effective diffusion coefficient. Here we analyze that equation for the simple case of hard spheres with a square well potential:

$$U(r) = \begin{cases} \infty & \text{if } r \le r_t \\ -\epsilon & \text{if } r_t \le r \le r_t + \lambda \\ 0 & \text{if } r \ge r_t, \end{cases} \tag{4}$$

where again $r_t = r_c + r_d$ is the sum of the hard-core radii of the crowder and the diffuser. Equation (4) of the article gives

$$0 = \int_0^\infty 4\pi r^2 \left(e^{-\beta U(r)} - 1\right) dr = -\frac{4}{3}\pi r_t^3 + (e^{\beta\epsilon} - 1)\int_{r_t}^{r_t+\lambda} 4\pi r^2 dr, \tag{5}$$

which in turn gives rise to

$$\epsilon_{\max} = k_B T \ln\left[\frac{(r_t+\lambda)^3}{(r_t+\lambda)^3 - r_t^3}\right] = k_B T \ln\left[\frac{(\frac{r_t}{\lambda}+1)^3}{(\frac{r_t}{\lambda}+1)^3 - (\frac{r_t}{\lambda})^3}\right] \tag{6}$$

This function is plotted in Fig. 8. The attraction strength $\epsilon_{\max}$ maximizing the diffusion rate exhibits a complex dependence on the ratio between the range r_t of the hard-core repulsion and the range λ of the attractive well. The dependence of $\epsilon_{\max}$ on this ratio is logarithmic when the ratio is large, suggesting that the non-monotonic dependence of the diffusion coefficient on ϵ may hold even for very large crowding obstacles. Series expansion shows that $\epsilon_{\max}$ is proportional to $(r_t/\lambda)^3$ when this ratio is small. Thus, the non-monotonic effect will be very difficult to observe for obstacles that are small compared to the attraction range. We note that using the values $\lambda = 0.5\,\mathrm{nm}$ and $r_t = 3 + 1 = 4\,\mathrm{nm}$ we find that $\epsilon_{\max} \approx 1.2$, close to the value of 1.4 obtained with the exponentially decaying potential used in the simulation.

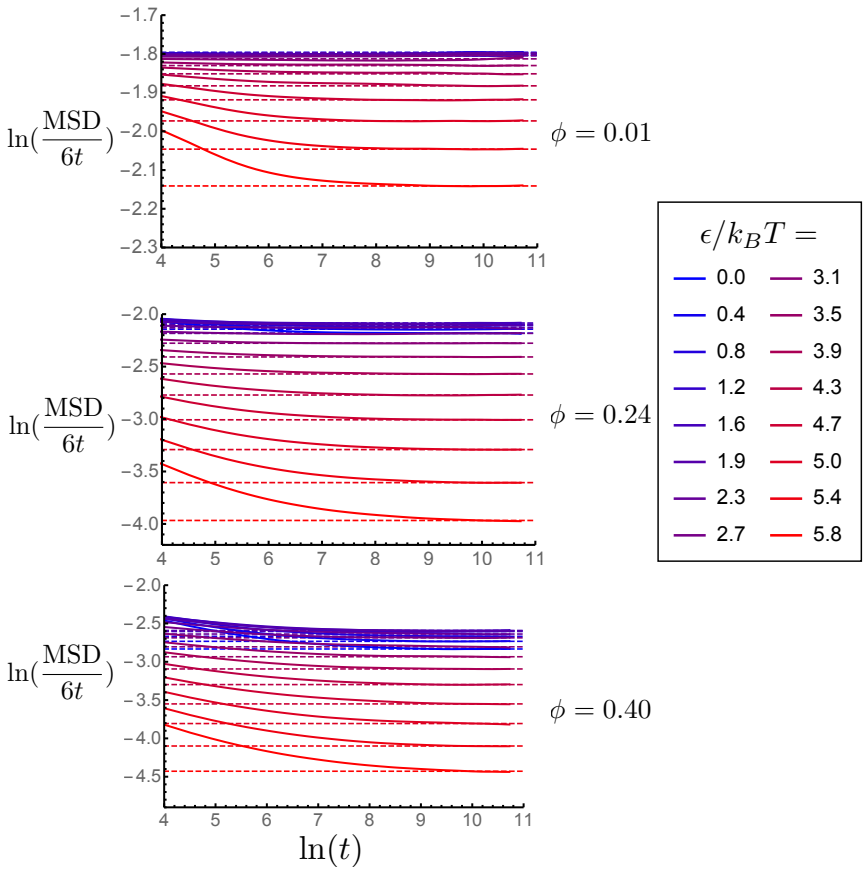

Figure 6: Logarithmic plots of MSD/$6t$ versus t for three different values of the crowder volume fraction ϕ, and for a range of values of the attraction strength ϵ. The dashed lines show the plateau values of ln(MSD/$6t$) to be used in the alternative method for calculating the effective diffusion coefficient.

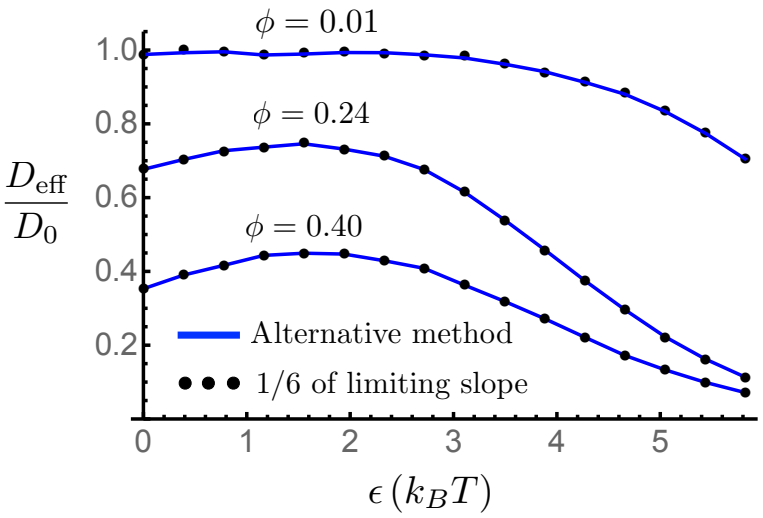

Figure 7: Selected diffusion coefficients calculated using the alternative method, compared to the method described in the article.

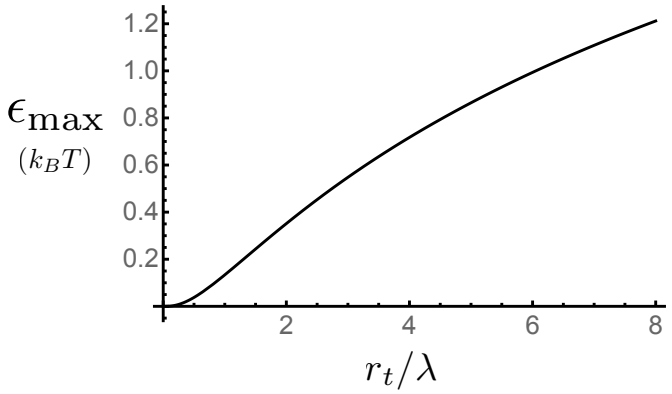

Figure 8: The value of ϵ_{max}, given by Eq. 6, which maximizes the diffusion rate, in the case of crowders with square-well attractive potentials. This is plotted as a function of the ratio of the hard-core radius r_t to the range λ of the attractive potential.

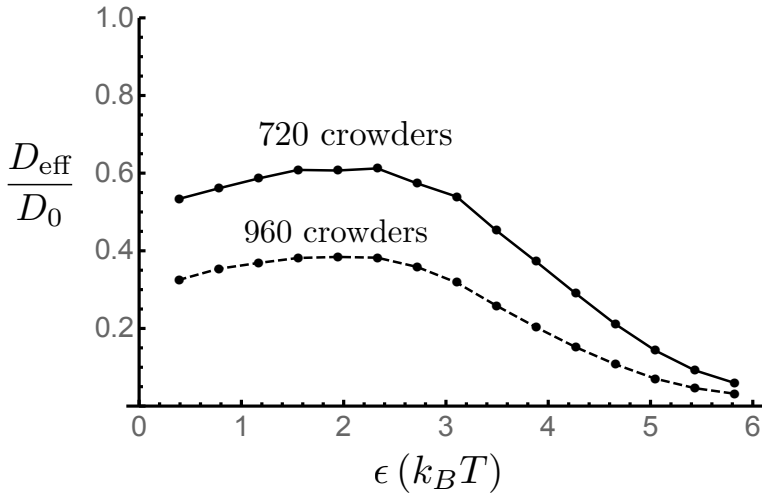

Figure 9: Effective diffusion coefficients calculated for a system in which the crowder-diffusion potential is given by a shifted Lennard-Jones potential. Crowder radius is 3 nm and diffuser radius 1 nm. The range of the LJ potential is $\sigma = 0.5\,\text{nm}$. The simulation box size is $70 \times 70 \times 70$ nm.

5 Lennard-Jones interactions

In order to verify that our main result (the non-monotonic dependence of D_{eff} on ϵ) does not depend on our particular choice of crowder-diffuser potential, we have performed simulations in which this interaction takes the form of a shifted Lennard-Jones (LJ) potential:

$$U(r) = U_{\text{LJ}}(r - r_t), \qquad \text{where} \tag{7}$$

$$U_{\text{LJ}}(r) = 4\epsilon\left[(\sigma/r)^{12} - (\sigma/r)^6\right] \tag{8}$$

Here $r_t = r_c + r_d$ is the sum of the hard-core radii of the crowder and diffuser. As in the article, we used crowders of radius 3 nm and diffusers of radius 1 nm, as well as a range $\sigma = 0.5\,\text{nm}$ of the LJ potential. Fig. 9 shows effective diffusion coefficients calculated from these simulations, showing the the non-monotonic dependence of D_{eff} on ϵ occurs also in this system. We note that the notion of the "volume occupied" by crowders is not precisely defined for this potential; for that reason Fig. 9 shows the number of crowders rather than their volume fraction.

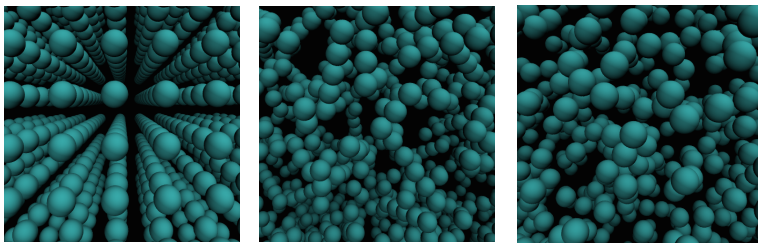

Figure 10: Illustration of different types of crowder configurations used. For clarity, a crowder volume fraction of $\phi = 0.08$ is shown. Illustrations were made using VMD (3).

6 Effect of crowder configuration

It is interesting to consider how our results may depend on the type of crowder configurations chosen. Three possibilities are shown in Fig. 10; for clarity these are shown at a relatively low crowder volume fraction of $\phi = 0.08$. The first is a regular cubic array or crystal of crowders. The second is what we call a "gel" configuration of crowders, and is produced as follows: A random location is chosen for the first crowder. The next crowders follow each other in a row or rod, advancing in a randomly chosen direction from the first crowder. This continues until an overlap occurs with a previously placed crowder (taking into account periodic boundary conditions). When an overlap occurs, a new location is chosen again and the process repeats until the desired number of crowders has been placed. A third type of crowder configuration, which we have used throughout the article, is a random configuration, that is, a configuration of crowders taken from an equilibrated simulation of only mobile crowders. We performed simulations using these three types of configuration, with a crowder volume fraction of $\phi = 0.24$. The results are shown in Fig. 11. Interestingly, the effective diffusion coefficient does not depend very strongly on the type of configuration used, especially for small values of ϵ. The non-monotonic dependence of D_{eff} on ϵ is also seen to be present in all three cases.

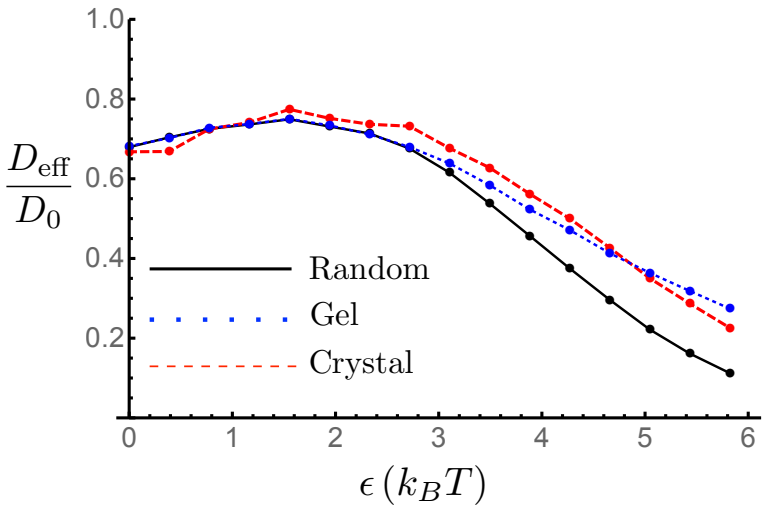

Figure 11: Effective diffusion coefficients calculated from simulations using crowder configurations of the three types depicted in Fig. 10. A crowder volume fraction $\phi = 0.24$ was used in all three cases.

7 Effect of crowder mobility

In the article we consider particles diffusing among fixed crowders. Here we examine the effect of crowder mobility on the effective diffusion coefficient of the diffusing 1 nm radius particles. Consistently with the Stokes-Einstein formula, we give the mobile crowders a mobility that is one third that of the diffusers. Fig. 12 shows our calculated effective diffusion coefficients for both fixed and mobile crowders, using a crowder volume fraction of $\phi = 0.24$. As could be expected, the particles diffuse faster among mobile crowders than among fixed ones. In the presence of mobile crowders, the non-monotonic dependence of D_{eff} on ϵ is weak compared to the case of fixed crowders. Fig. 13 shows the same thing for a higher crowder volume fraction of $\phi = 0.32$, and also includes simulation data for the case of an equal mixture of fixed and mobile crowders, showing a smooth interpolation between the cases of fixed or mobile crowders only. At this higher volume fraction, the non-monotonic effect, although weak, is still clearly discernible.

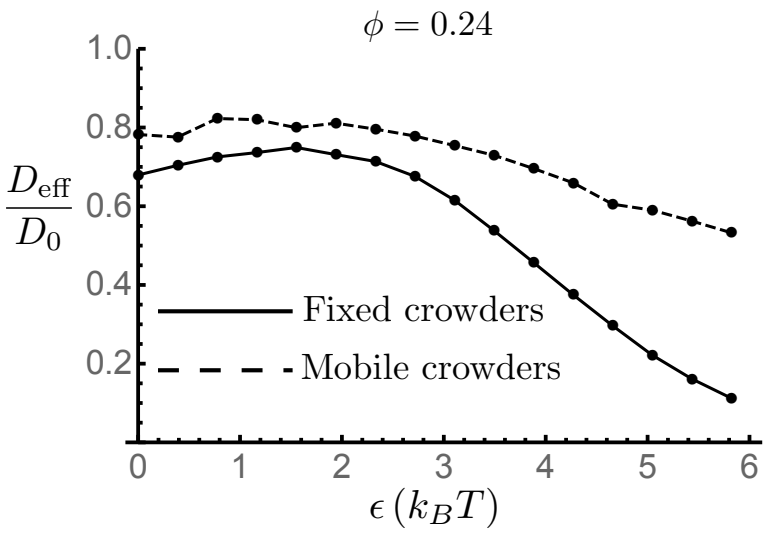

Figure 12: Comparison of effective diffusion coefficients of diffusers in the case of fixed versus mobile crowders. A crowder volume fraction $\phi = 0.24$ was used in both cases.

8 Variation of crowder size

In order to study the effect of varying the size of the crowders, we have performed simulations with crowders of different hard-core radii, namely $r_c = 6$ nm and $r_c = 1.5$ nm in addition to the 3 nm radius crowders considered in the article. Fig. 14 shows the results of three sets of simulations, all using the same volume fraction $\phi = 0.24$ of crowders and the same characteristic range $\lambda = 0.5$ nm of the attractive potential. The non-monotonic dependence of D_{eff} on ϵ is visible in all three cases, although it is seen to be a relatively stronger effect for small crowders. We note also that the attraction strength, $\epsilon_{\max}$, which maximizes the diffusion rate, increases as a function of the crowder size, consistently with the considerations in section 4 of the Supplementary Materials.

9 Diffusing polymers

The non-monotonic dependence of D_{eff} on ϵ may depend greatly on the internal degrees of freedom of the diffusing molecule. To investigate this,

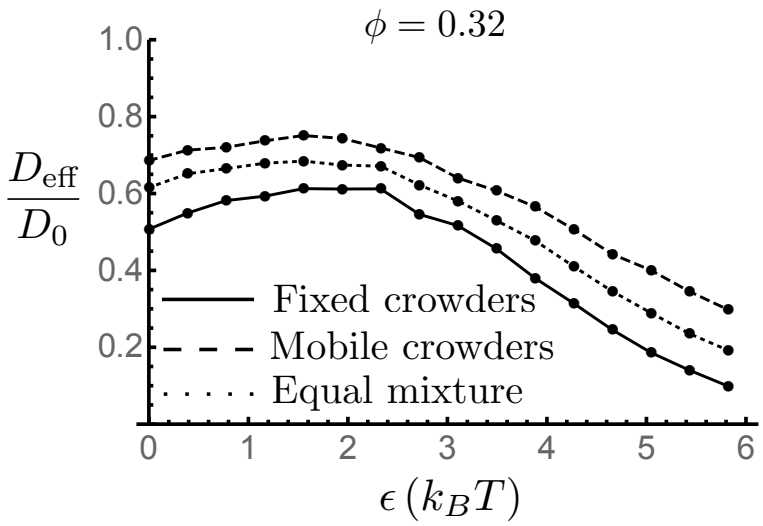

Figure 13: Comparison of effective diffusion coefficients of diffusers for three cases: fixed crowders (solid line), mobile crowders (dashed), and an equal mixture of fixed and mobile crowders (dotted). A crowder volume fraction $\phi = 0.32$ was used in both cases.

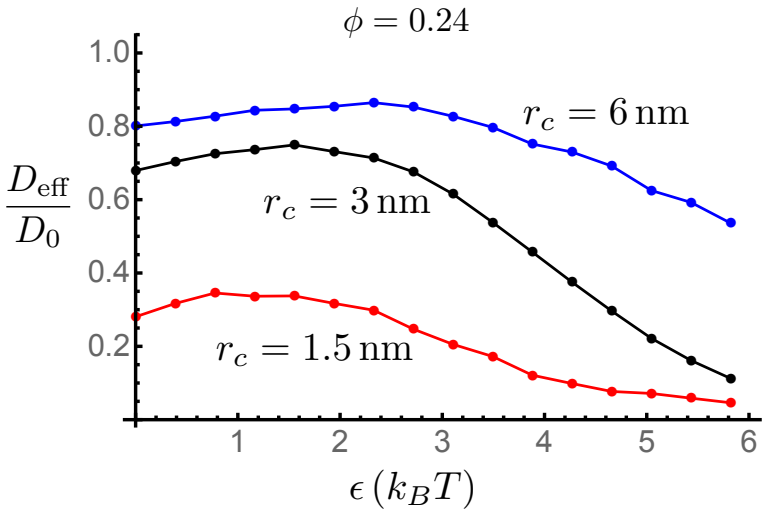

Figure 14: Effective diffusion coefficients in the presence of crowders of different radii. Top: $r_c = 6.0\,\text{nm}$. Middle: $r_c = 3.0\,\text{nm}$. Bottom: $r_c = 1.5\,\text{nm}$. A crowder volume fraction $\phi = 0.24$ was used in all three cases.

we performed simulations of short polymers diffusing among the same fixed crowders as in the article. Each polymer consists of 5 monomers identical to the diffusing particles considered in the article, including interactions with crowders. Neighboring monomers interact via a potential that constrains the distance between their centers to be very nearly 2.0 nm; no stiffness (angle) potentials were used. The inset of Fig. 15 shows one of these polymers as well as the surrounding crowders. The plot in Fig. 15 shows a striking non-monotonic dependence of the polymer's diffusion coefficient on the strength ϵ of the monomer-crowder attraction. As might be expected, the position of the maximum occurs at a smaller value of ϵ than in the case of diffusing monomers. Even more importantly, the overall increase in diffusion rate as the attractive interaction is turned on is large, of order 50 percent.

10 Alternative method for calculation of μ^{cell}

In the article, the roughness of the excess chemical potential landscape was quantified by calculating the effective potential (Eq. 2 of the article) for each cell. The roughness was then given by the population standard deviation across all cells. This method used only the potential generated by the fixed

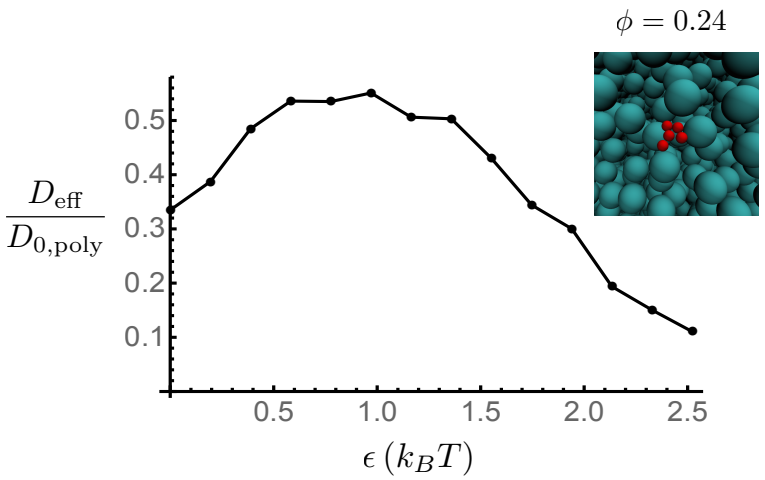

Figure 15: Effective diffusion coefficient of a polymer ($n = 5$ monomers) diffusing among fixed crowders. The diffusion coefficients are normalized by the "bare" diffusion coefficient of the polymer in the absence of any obstacles, $D_{0,\text{poly}} = D_0/n$. Inset: snapshot made using VMD (3).

configuration of crowders. Since it amounts to a direct evaluation of the partition function in Eq. (2) of the article, this method should be exact, assuming accurate numeric integration.

Direct evaluation of the partition function is possible here because we only need to integrate over the position of the single diffusing particle. This is not possible in systems with many interacting degrees of freedom (for example, the same system but with mobile crowders). In those cases, the only way to calculate the excess chemical potential landscape is directly from the simulation trajectories, often using histograms of various order parameters. It is interesting to perform the same type of calculation for our system and to compare the results to those given directly by partition function.

We take as our order parameter the position of the diffusing particle, binned according the the division of the system into $14 \times 14 \times 14$ nm cells. From a simulation trajectory, we can calculate the probability p_i^{cell} that a diffusing particle occupies cell i. The free energy change for moving the diffusing particle from cell i to cell j is $-k_BT \cdot \ln(p_i^{\text{cell}}/p_j^{\text{cell}})$. This is also the chemical potential difference between these cells. It follows that the roughness of the chemical potential landscape, in units of k_BT, can be calculated

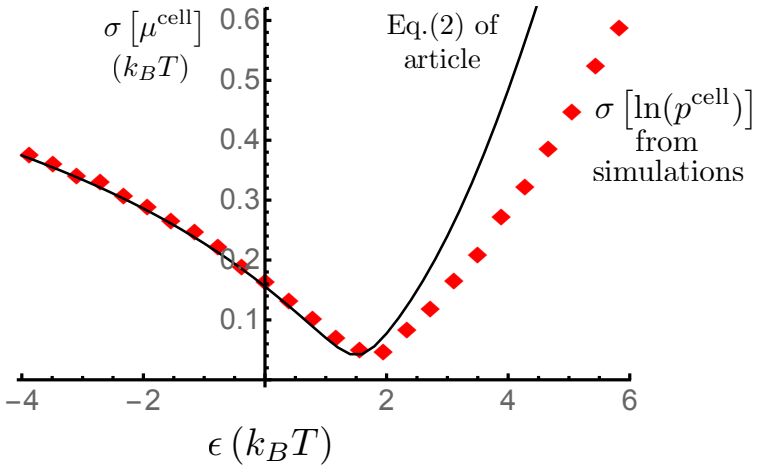

Figure 16: Comparison of two methods of calculating the roughness of the chemical potential landscape for a system with crowder volume fraction $\phi = 0.24$. Black curve: μ^{cell} calculated as explained in the article, using only the crowder configuration. Red diamonds: standard deviation of $\ln(p^{\text{cell}})$ calculated using only simulation trajectories as explained in SM section 10. In both cases the $70\times70\times70$ nm system volume was divided into $14\times14\times14$ nm cells.

as

$$\sigma\left[\ln(p^{\text{cell}})\right] = \sqrt{\frac{1}{N_{\text{cells}}}\sum_i (\ln(p_i^{\text{cell}}) - \overline{\ln(p^{\text{cell}})^2}} \tag{9}$$

We note that this method, which uses only the simulation trajectory, is complementary to the one used in the article, which uses only the spatially varying potential generated by the crowders.

Fig. 16 shows a comparison of the two methods for calculating the roughness of the chemical potential landscape. In both cases, the same discretization of the system into $14 \times 14 \times 14$ nm cells is used.

11 Determination of D_{eff} from the Fokker-Planck equation

Here we show that the main conclusion of the paper, the non-monotonicity of D_{eff} as a function of ϵ, can be derived from the equations that describe the probability flux of the diffuser (i.e. the Fokker-Planck equations). This field-based approach is completely different from the Brownian Dynamics simulation approach described in the main text.

We consider the diffusion of a single diffuser in the presence of fixed crowders. In equilibrium, the probability flux at any point in the system is zero. If a biasing force $\vec{F}$ is imposed on the system, a net probability flux develops, given by:

$$\vec{J}(\vec{r}) = -D_0\vec{\nabla}\rho(\vec{r}) - D_0\rho(\vec{r})\vec{\nabla}\beta U(\vec{r}) + D_0\rho(\vec{r})\vec{F}, \tag{10}$$

where $\rho(\vec{r})$ is the probability density of the diffuser, D_0 is its microscopic diffusion coefficient in the absence of forces or obstacles, and $U(\vec{r})$ is the total potential created by the crowders at $\vec{r}$, including both hard-core repulsions and short-range attractions. More specifically, $U(\vec{r})$ is given by the sum of all crowder-diffuser pairwise interactions, given by Eq. 1 of the main text.

The probability density $\rho(\vec{r})$ is normalized:

$$\int \rho(\vec{r})d\vec{r} = 1, \tag{11}$$

where the integral runs over the volume of the whole system. In the steady state, the probability flux fulfills the continuity condition:

$$\vec{\nabla} \cdot \vec{J}(\vec{r}) = 0 \tag{12}$$

Let us consider a macroscopic picture of the system (see Figure 17a), where we discretize the space in cells of volume V. The size of the cells is chosen such that they all have the same average probability density and potential. In this macroscopic picture, the probability flux in the direction of $\vec{F}$ is:

$$J = D_{\text{eff}}\rho F, \tag{13}$$

where F is the modulus of $\vec{F}$ and ρ is the average probability density in the cell,

$$\rho = \frac{\int_V \rho(\vec{r})d\vec{r}}{V} \tag{14}$$

Without loss of generality, we will assume that $\vec{F}$ is normal to one of the sides of the cell (red line in Figure 17a). The total current obtained by integrating Eq. 10 (microscopic picture) on one of the sides normal to $\vec{F}$ produces the same total current as that obtained by integrating Eq.13 (macroscopic picture). Therefore:

$$\int \vec{J}(\vec{r}) \cdot \vec{n}\, dA = D_{\text{eff}} \rho F A, \tag{15}$$

where A is the area of the side of the cell and $\vec{n}$ is a unit vector normal to the side of the cell. Thus,

$$D_{\text{eff}} = \frac{\int \vec{J}(\vec{r}) \cdot \vec{n}\, dA}{\rho F A} \tag{16}$$

Note that the $\rho(\vec{r})$ in Eq. 10 is a steady-state probability density and is therefore different from the equilibrium probability density sampled in the BD simulations, $\rho^{\text{eq}}(\vec{r})$. However, in the limit $F \to 0$, $\rho(\vec{r}) \to \rho^{\text{eq}}(\vec{r})$, so we calculate

$$D_{\text{eff}} = \lim_{F \to 0} \frac{\int \vec{J}(\vec{r}) \cdot \vec{n}\, dA}{\rho F A} \tag{17}$$

In order to determine D_{eff}, we need to solve Eqs. 10 and 12 in the whole system under the constraint of normalization (Eq. 11). Performing such a calculation in three dimensions for a system with more than a few randomly distributed crowders is computationally prohibitive. However, we can consider the case where the crowder distribution is symmetric and use symmetry considerations in the calculations. We will consider, therefore, a cubic array of crowders (i.e. the crystal structure in Figure 10). We observed that BD simulations for that system display a non-monotonic behavior of $D_{\text{eff}}(\epsilon)$ similar to that observed for randomly distributed crowders. We solved the system of differential equations 10, 11 and 12 in this system using Finite Elements with the software Comsol Multiphysics 4.3b. Figure 18 shows that the D_{eff}/D_0 versus ϵ plot presents a maximum for a positive value of ϵ ($\epsilon = 1.3\, k_B T$), in agreement with the behavior observed in BD simulations.

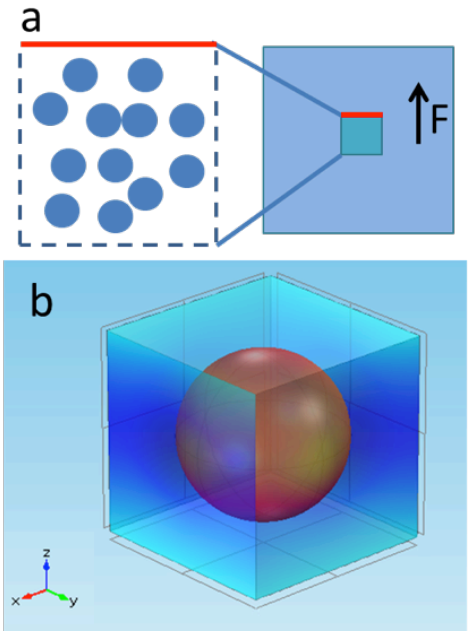

Figure 17: a. Scheme showing the diffusion equation-based approach to determine D_{eff}. We consider the diffusion of the diffuser probability both at the microscopic level where the system is inhomogeneous (left) and at the macroscopic level where we partition the system into cells (small square in the right panel), such that the system is effectively homogeneous at the coarse-grained scale. We impose a drift force and determine the probability flux across a surface normal to this force (red line) b. Cell used in the Finite Element calculations. We consider a cell with periodic boundary conditions in the three spatial directions. The drift force is applied in the z direction. The central crowder interacts with the diffuser according Eq. 1 in the main text with $\lambda = 0.5$ nm. The crowder has radius $r_c = 3$ nm and the box has a side of 12 nm, which results in a crowder volume fraction $\phi = 0.065$.

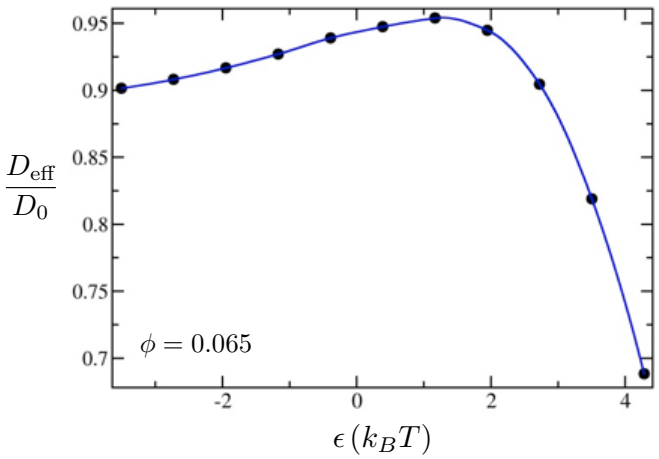

Figure 18: D_{eff}/D_0 determined from probability diffusion calculations as a function of the strength ϵ of the crowder-diffuser attractions.

References

[1] Saxton, M., 1993. Anomalous Diffusion Due to Obstacles: A Monte Carlo Study. *Biophys J* 66:394–401.

[2] Vilaseca, E., A. Isvoran, S. Madurga, I. Pastor, J. Garc'es, and F. Mas, 2011. New insights into diffusion in 3D crowded media by Monte Carlo simulations: effect of size, mobility and spatial distribution of obstacles. *Phys. Chem. Chem. Phys.* 13:7396–7407.

[3] Humphrey, W., A. Dalke, and K. Schulten, 1996. VMD: Visual Molecular Dynamics. *J. Mol. Graphics* 14:33–38.